Image Compression with Embedded Multiwavelet Coding

Kai-Chieh Liang, Jin Li and C.-C. Jay Kuo

Signal and Image Processing Institute and Department of Electrical Engineering-Systems
University of Southern California, Los Angeles, California 90089-2564

ABSTRACT

An embedded image coding scheme using the multiwavelet transform and inter-subband prediction is proposed in this research. The new proposed coding scheme consists of the following building components: GHM multiwavelet transform, prediction across subbands, successive approximation quantization, and adaptive binary arithmetic coding. Our major contribution is the introduction of a set of prediction rules to fully exploit the correlations between multiwavelet coefficients in different frequency bands. The performance of the proposed new method is comparable to that of state-of-the-art wavelet compression methods.

Keywords: Embedded image coding, multiwavelets, interband prediction.

1 INTRODUCTION

A novel image coding algorithm known as the embedded zerotree wavelet (EZW) method was recently proposed by Shapiro [4]. A scalar wavelet transform is first performed, and then a successive approximation quantization (SAQ) scheme was adopted to generate a bit stream in the order of importance. Furthermore, by exploiting the fact that when a zero symbol appears in the coarser level, it is likely that zeros will also appear in the same spatial locations of the corresponding finer scales, Shapiro developed a prediction rule called the zerotree prediction to reduce the redundancy among wavelet coefficients in different scales.

One new development in wavelet research is the design and analysis of multiwavelets. Multiwavelets differ from scalar wavelets in that two or more scaling functions and mother wavelets are used for signal representation. One famous multiwavelet filter is the GHM filter proposed by Geronimo, Hardin, and Massopust [1] [2]. The GHM basis offers a combination of orthogonality, symmetry, and compact support, which cannot be achieved by any scalar wavelet basis except for the Haar basis [7].

In this work, we are interested in the generalization of the Shapiro's algorithm to the context of multiwavelet transform. It turns out that the prediction rule has to be greatly modified so that the redundancy between wavelet coefficients can be effectively removed. There are two major differences in our prediction scheme. First, prediction has to be performed before quantization while prediction is performed after quantization in EZW. Thus, our prediction has to be supplemented by residual coding. Second, prediction only applies to insignificant symbols (zerotree) in EZW while prediction works for both significant and insignificant symbols in our new setting.

This paper is organized as follows. A brief review of multiwavelet theory is presented in Section 2. The new prediction rule among wavelet coefficients is described in Section 3, and the new proposed coding scheme is given in Section 4. Experimental results are provided in Section 5. Concluding remarks and possible extensions are stated in Section 6.

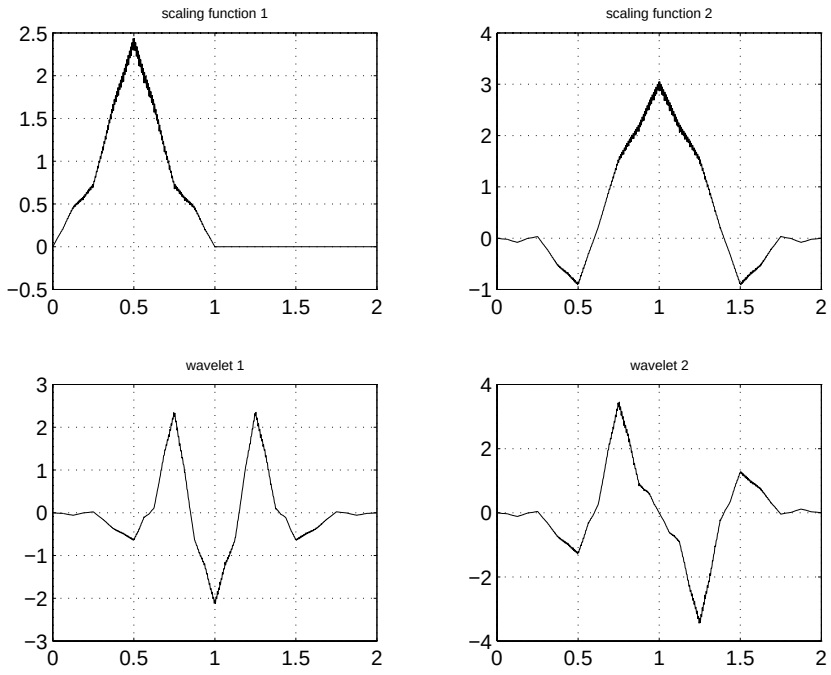

Figure 1: The two scaling (up) and two mother wavelet (down) functions of the GHM multiwavelet filter.

	multiwavelet	DB 8 tap	9-7 tap	Haar
Orthogonality	yes	yes	no	yes
Symmetry	yes	no	yes	yes
compact support	yes	yes	yes	yes

Table 1: Property comparison of several wavelet filters.

2 Review of Multiwavelet Filter

Multiwavelets have two or more scaling functions and mother wavelets for signal representation. To give an example, the scaling and mother wavelet functions of the GHM filter [1] [2] are plotted in Fig. 1. The properties of the GHM multiwavelet filter and scalar filters are listed in Table 1.

To implement the multiwavelet transform, we require a new filter bank structure where the lowpass and highpass filter banks are matrices rather than scalars. That is, the two scaling and wavelet functions satisfy the following two-scale dilation equations [3]:

$$\begin{bmatrix} \phi_1(t) \\ \phi_2(t) \end{bmatrix} = \sqrt{2} \sum_k H_k \begin{bmatrix} \phi_1(2t-k) \\ \phi_2(2t-k) \end{bmatrix}, \tag{1}$$

and

$$\begin{bmatrix} \psi_1(t) \\ \psi_2(t) \end{bmatrix} = \sqrt{2} \sum_k G_k \begin{bmatrix} \psi_1(2t-k) \\ \psi_2(2t-k) \end{bmatrix}, \tag{2}$$

where

$$\begin{aligned} H_0 &= \sqrt{2} \begin{bmatrix} 3/10 & 2\sqrt{2}/5 \\ -\sqrt{2}/40 & -3/20 \end{bmatrix} \quad H_1 = \sqrt{2} \begin{bmatrix} 3/10 & 0 \\ 9\sqrt{2}/40 & 1/2 \end{bmatrix} \\ H_2 &= \sqrt{2} \begin{bmatrix} 0 & 0 \\ 9\sqrt{2}/40 & -3/20 \end{bmatrix} \quad H_3 = \sqrt{2} \begin{bmatrix} 0 & 0 \\ -\sqrt{2}/40 & 0 \end{bmatrix}, \end{aligned} \tag{3}$$

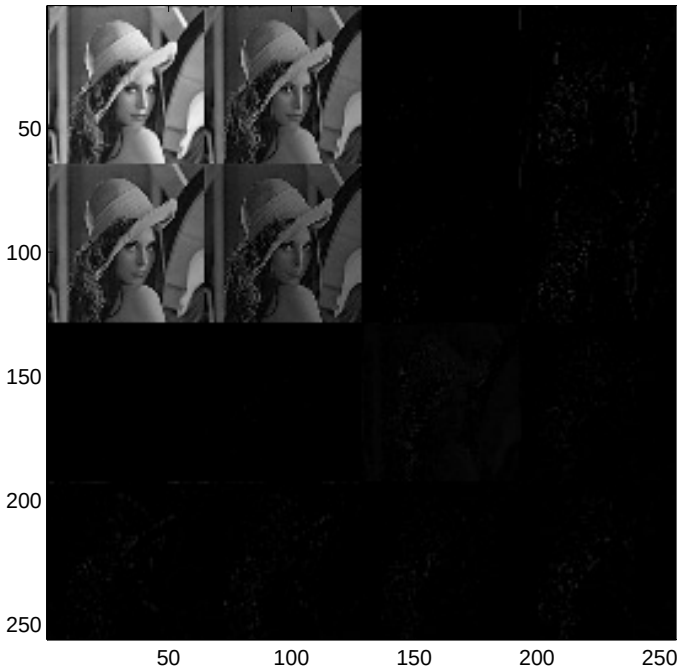

Figure 2: Multiwavelet transform of the Lena image.

and

$$G_0 = \sqrt{2}\begin{bmatrix} -\sqrt{2}/40 & -3/20 \\ -1/20 & -3\sqrt{2}/20 \end{bmatrix} \quad G_1 = \sqrt{2}\begin{bmatrix} 9\sqrt{2}/40 & -1/2 \\ 9/20 & 0 \end{bmatrix}$$
$$G_2 = \sqrt{2}\begin{bmatrix} 9\sqrt{2}/40 & -3/20 \\ -9/20 & 3\sqrt{2}/20 \end{bmatrix} \quad G_3 = \sqrt{2}\begin{bmatrix} -\sqrt{2}/40 & 0 \\ 1/20 & 0 \end{bmatrix}. \tag{4}$$

Since the GHM filter has two scaling and two wavelet functions, it has two lowpass subbands and two highpass subbands in the transform domain. We show in Fig. 2 the Lena image of size 256×256 after the GHM multiwavelet transform as an example. The transformed Lena image has in each dimension two low frequency and two high frequency sub-images. It is easy to see that there are similarities between low frequency sub-images so that it is possible to apply a certain prediction rule to remove the redundancy between these subbands.

The scalar wavelet transform can be written in terms of the matrix form as:

$$\begin{bmatrix} h_0 & h_1 & h_2 & h_3 & \cdots & \cdots & \cdots \\ g_0 & g_1 & g_2 & g_3 & \cdots & \cdots & \cdots \\ 0 & 0 & h_0 & h_1 & h_2 & h_3 & \cdots \\ 0 & 0 & g_0 & g_1 & g_2 & g_3 & \cdots \\ \cdots & \cdots & \cdots & \cdots & \cdots & \cdots & \cdots \end{bmatrix}, \tag{5}$$

where h_i and g_i are the low- and high-pass filter impulse responses. In contrast, the vector wavelet transform can

be written as:

$$\begin{bmatrix}
h_{0,0} & h_{0,1} & h_{0,2} & h_{0,3} & \cdots & \cdots & \cdots & \cdots & \cdots \\
h_{1,0} & h_{1,1} & h_{1,2} & h_{1,3} & \cdots & \cdots & \cdots & \cdots & \cdots \\
g_{0,0} & g_{0,1} & g_{0,2} & g_{0,3} & \cdots & \cdots & \cdots & \cdots & \cdots \\
g_{1,0} & g_{1,1} & g_{1,2} & g_{1,3} & \cdots & \cdots & \cdots & \cdots & \cdots \\
0 & 0 & 0 & 0 & h_{0,0} & h_{0,1} & h_{0,2} & h_{0,3} & \cdots \\
0 & 0 & 0 & 0 & h_{1,0} & h_{1,1} & h_{1,2} & h_{1,3} & \cdots \\
0 & 0 & 0 & 0 & g_{0,0} & g_{0,1} & g_{0,2} & g_{0,3} & \cdots \\
0 & 0 & 0 & 0 & g_{1,0} & g_{1,1} & g_{1,2} & g_{1,3} & \cdots \\
\cdots & \cdots & \cdots & \cdots & \cdots & \cdots & \cdots & \cdots & \cdots \\
\cdots & \cdots & \cdots & \cdots & \cdots & \cdots & \cdots & \cdots & \cdots
\end{bmatrix} \tag{6}$$

By examining the transform matrices of the scalar wavelet and multiwavelet as shown in Equations 5 and 6, respectively, one can see that in the multiwavelet transform domain that there are first and second lowpass coefficients followed by first and second high pass filter coefficients rather than one lowpass coefficient followed by one highpass coefficient. Therefore, if we separate these four coefficients, there are four subbands in the transform domain.

3 Inter-band Prediction

To demonstrate the inter-band correlation, let us perform the GHM filtering on an ideal sine function and a randomly selected line of the Lena image. The correlations between (L1,L2), (L1,H1), and (L1,H2) subbands are shown in Figs. 3 and 4, where each point represents the wavelet coefficient values in the same spatial location of two corresponding bands. For the sine signal, there are linear relationships between the wavelet coefficient values for the subband pairs (L1,L2) and (L1,H1) but not for the subband pair (L1,H2). For the real signal, the observation is approximately valid with a few outlying points. By performing a linear regression on the data points, we can obtain a prediction model as:

$$\begin{aligned} L2 &= -0.6569 \times L1, \\ H1 &= +0.2010 \times L1. \end{aligned}$$

The above prediction rules can be explained as follows. For most natural images, multiwavelet subbands L2 and H1 have very strong low frequency components so that the energy is concentrated in the neighborhood of the DC region. One typical example is given in Fig. 5. Thus, to understand why the symbol in L1 subband can predict the magnitude of symbols in L2 and H1 subbands up to a very high percentage, we are in fact analyzing whether the magnitude of the DC symbol in the L1 suband can predict those in the L2 and H1 subbands.

Let us examine the frequency responses of the GHM multiwavelet filters as shown in Fig. 6, where the frequency response of band L1 was overlaid on those of bands L2, H1 and H2. We see that L1, L2 and H1 do not vanish at the zero frequency so that these three filters all share a portion of the DC component. Since that the magnitude of low frequency coefficient in each subband is amplified by the value of the filter response at the zero frequency, it is reasonable to expect that the prediction ratio between L1 and L2 is the ratio of the magnitudes of the DC components of filters L1 and L2. It turns out that the ratio of filter magnitudes between L2 and L1 is 0.6569, which happens to be identical to the coefficient given by the linear prediction rule. Similarly, the ratio of the magnitudes of the DC components in band H1 and L1 is 0.2010, which is again consistent with the empirical prediction rule stated above. It is also worthwhile to point out that filter H2 has a zero value at the DC component so that it does have any share of the DC signal. Thus, we are not able to predict its value.

One may wonder if this subband prediction rule also exists in the scalar wavelet case. The answer is no. We show the frequency response of the Daubechies 8-tap filter in Fig. 7. It is obvious that DC signals can hardly pass high pass filter. The ratio of the magnitude of low frequency signal in the high frequency subband and that in the low frequency subband is almost zero. In other words, lowpass and highpass filters are highly decorrelated at the low frequency region.

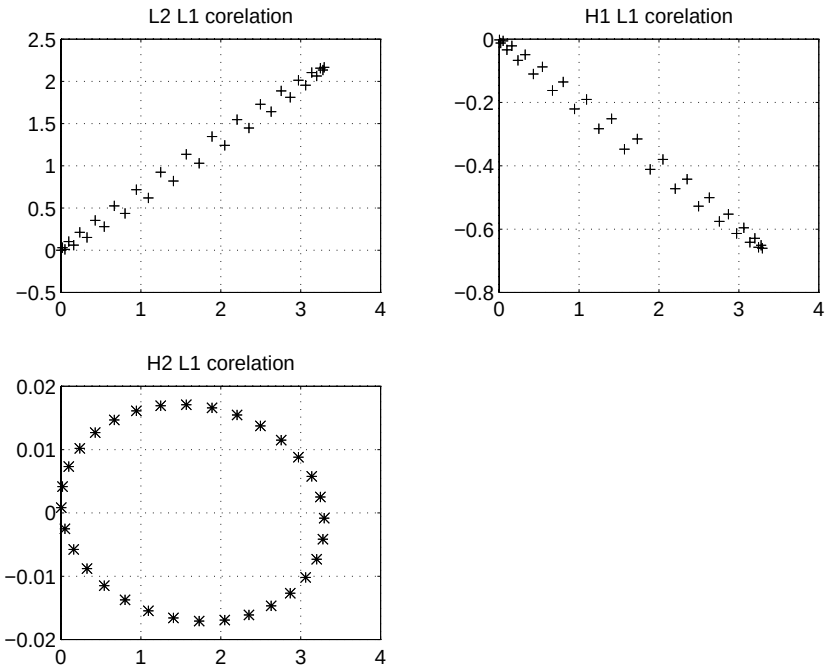

Figure 3: Correlations of the multiwavelet coefficients of a sine signal.

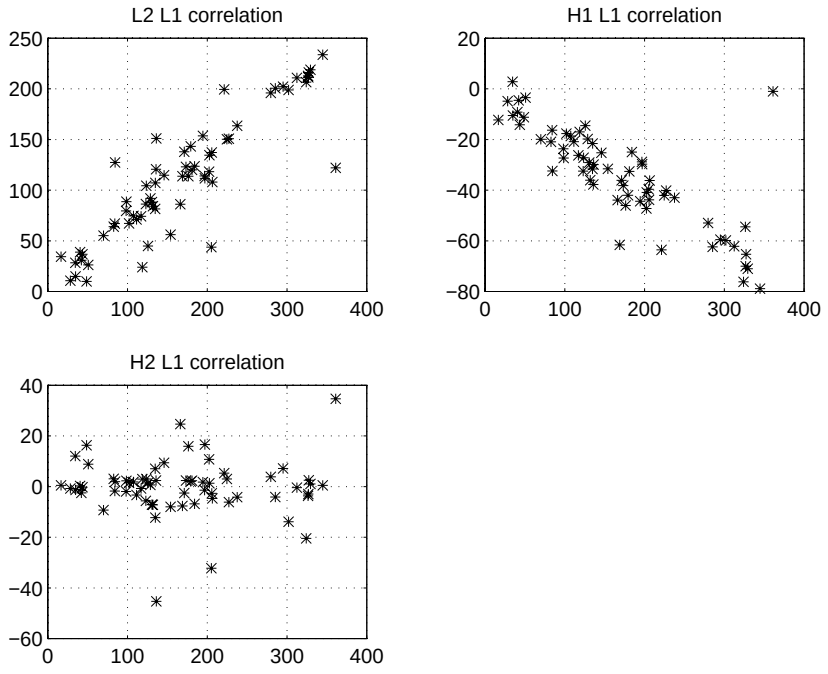

Figure 4: Correlations of the multiwavelet coefficients of the 55th row of the Lena image.

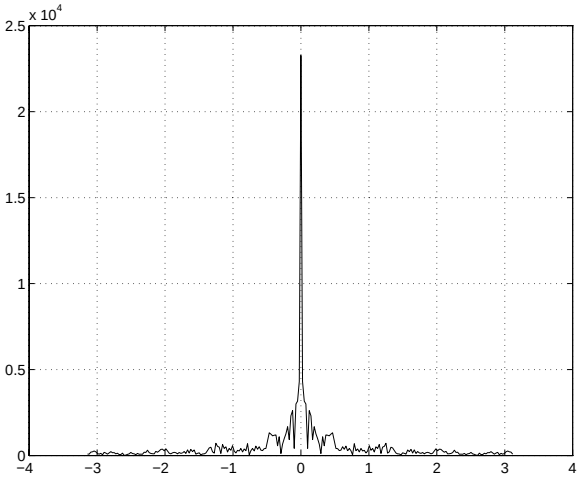

Figure 5: A typical plot of transform coefficient magnitudes in a wavelet subband.

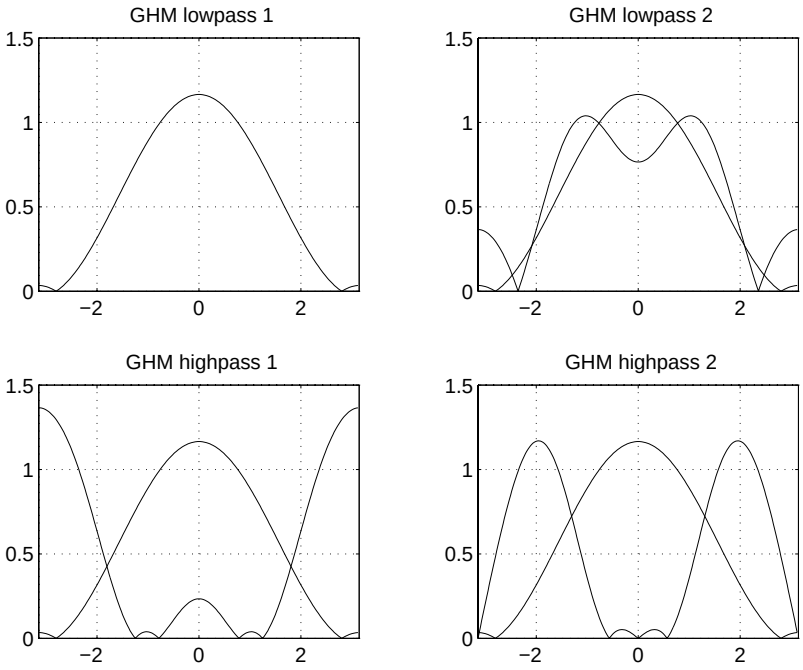

Figure 6: Frequency responses of the GHM filters, where the frequency response of band L1 is shown in the left-upper corner and it is overlaid on those of bands L2, H1 and H2 in the other three figures.

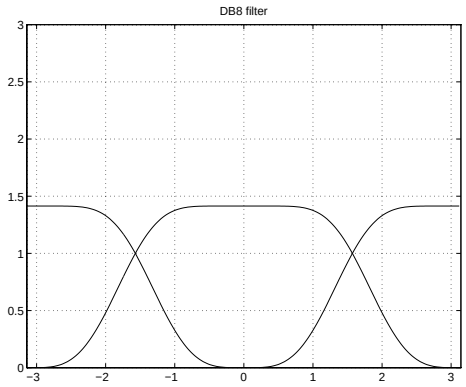

Figure 7: The lowpass and highpass filter frequency responses of the Daubechies 8-tap filter.

Our prediction rule can be viewed as a variation of DPCM in the JPEG standard, where the DC term is picked up from each DCT block and encoded by DPCM. That is, the first DC term is used as an estimate value for the second DC term, the second one as an estimate value for the third one, and etc. The DC predictions are across DCT blocks. In multiwavelet transform, the DC components fall in bands L1, L2 and H1 and can be predicted accordingly.

4 PROPOSED NEW CODING METHOD

Our coding scheme is composed by the following concepts:

1. GHM multiwavelet transform
2. inter-subband prediction
3. successive approximation quantization (SAQ)
4. adaptive binary arithmetic coding.

The GHM transform provides the possibility to use the magnitude of a symbol in one subband to predict that in another subband. Due to this property, our coding scheme performs prediction before quantization, in contrast with the prediction after quantization scheme used in EZW. After each transform, inter-subband or intra-subband prediction rules are applied to the wavelet coefficients. Inter-subband predictions are the linear predictions between L1 and L2, and between L1 and H1 subbands. Intra-subband predictions are the DPCM within the L1 subband. Both predictions are basically DC signal predictions, and energy of subbands can be greatly reduced by using this concept. For quantization and coding, we use the successive approximation quantization and adaptive binary arithmetic coder as proposed in LZC [5]. LZC [6] uses one symbol along the same spatial location in the parent subband, one from grand parent subband, and four symbols in the neighborhood as coding context of binary arithmetic coder. Here, since we have exploited the similarities between subbands in the prediction stage, the context of coder is defined by four symbols in the neighborhood only. No other symbols outside the subband are used in the context.

Our new coding scheme differs from EZW or LZC in several aspects. First, EZW and LZC use Daubechies seven-nine tap scalar filter, which is symmetric but not orthogonal. The seven-nine filter was chosen because of its high transform efficiency and high energy compaction. Our transform filter is the GHM multiwavelet filter. Even though GHM does not have a high energy compaction ratio as the seven-nine filter, it has both orthogonality and symmetry. Second, the zerotree prediction is used in EZW and applied after successive approximation quantization. Our prediction rule predicts the magnitude of symbols across two low frequency subbands or across low and high frequency subbands. The prediction is applied before quantization.

5 EXPERIMENTAL RESULTS

We use experiments to verify the accuracy of the prediction model in Section 5.1, and show a preliminary image compression result in Section 5.2.

5.1 Verification of Inter-band Prediction

Two experiments are considered in this subsection. The first experiment compares the subband energy, energy compaction between GHM (ghm), GHM with subband prediction (pghm), and the Daubechies 8-tap filter (db8). The relative prediction error is also checked. Another experiment is to check the magnitude profile of the wavelet coefficients with pghm and db8.

For simplicity, both the source signal and wavelet transform are chosen to be one-dimensional only. Each row of the Lena image of size 256×256 is used as the 1-D test signal. Thus, there are totally 256 test signals. A one-level 1-D multiwavelet transform is performed on each test signal so that there are four multiwavelet (ghm) subbands in the transform domain: first lowpass (L1), second lowpass (L2), first highpass (H1) and second highpass (H2) and each of L1, L2, H1 and H2 has 64 symbols. Then, the symbol in the L1 subband is used to predict those in L2 and H1 subbands. We also perform two-level Daubechies 8-tap filter (db8) on the 1-D test signals. After the transform, there are three wavelet subbands - first level lowpass subband (L1), first level highpass subband (H1), and zeroth level highpass subband (H0), where subbands L1 and H1 have 64 symbols and subband H0 has 128 symbols. Then, we do the following comparison on energy compaction:

- L1 of ghm is compared with L1 of db8,
- L2 of ghm is compared with H1 of db8,
- H1 and H2 of ghm are compared with H0 of db8.

The energy compaction ratios of the 256 test signals are plotted in Fig. 8 and the mean values of the ratios are given in Table 2. One can see from Table 2 that ghm L1 and L2 bands take approximately 66.95% and 29.74% of the total energy, respectively. After inter-band prediction, the ratio of pghm L2 and H1 are decreased to 3.27% and 0.43%, respectively, and that of L1 is increased to 95.65%. Thus, it is clear that most of the energy in the ghm L2 and H1 subbands are successfully removed by prediction.

By carefully examining Fig. 8, we find that the energy ratios of pghm L1 subband are lower between the 100th and 200th rows of the Lena image. This is because that the prediction model cannot successfully predict the high frequency hair textures in this region. The same reason explains why the ratios of pghm L2 and H1 are higher between the 100th and 200th rows. Fig. 8 also shows that db8 filter has a higher energy ratio in the L1 subband and a lower energy ratio in the H1 band for every test signal. The difference between db8 and pghm increases as the region contains more textures. This implies that prediction may not be as efficient as transform. Unless some other method is devised to reduce the ratios of pghm L2, our coding scheme has to pay more bits to encode the pghm L2 subband than db8 H1 subband.

We plot the Lena image after the GHM multiwavelet transform and inter-band prediction in Fig. 9. The difference between with and without prediction can be clearly seen by comparing Fig. 2 and Fig. 9. The energy left in the L2 and H1 subbands are all high frequency components. The original second low frequency Lena sub-images in Fig. 2 have been removed, and only the edges are left in the subbands.

The mean values of subband energies of ghm, pghm, and db8 are summarized in Table 3. We see from this table that the energy values of pghm L2 and H1 subbands are reduced to 7.65% and 10.42% of those without prediction, respectively. Furthermore, pghm has only 70% of the total energy of ghm. The energy reduction comes from a one level 1-D transform and prediction. With a 2-D transform and prediction, energy can be reduced up to 50%. More energy reduction can be achieved by applying more levels of multiwavelet transforms and predictions.

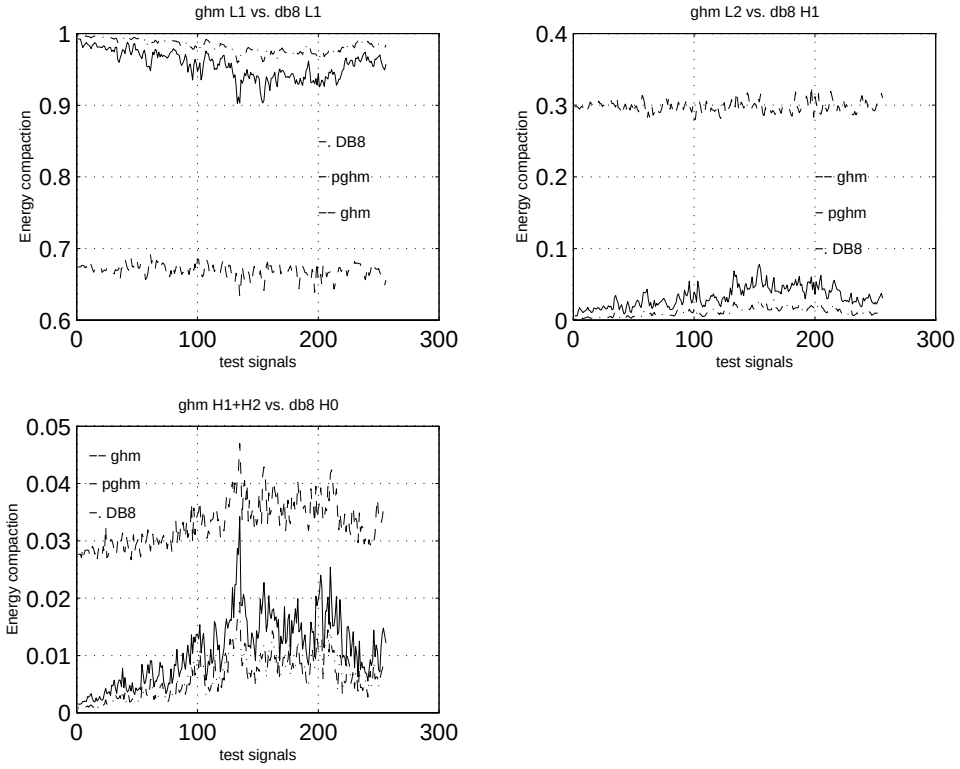

Figure 8: Energy compaction ratios of ghm, pghm, and db8 filters.

Energy compaction	L1	L2	H1	H2
ghm	0.6695	0.2974	0.0285	0.0046
pghm	0.9565	0.0327	0.0043	0.0065

Energy compaction	L1	H1	H0
db8	0.9827	0.0111	0.0062

Table 2: Mean values of subband energy compaction ratios of ghm, pghm, and db8.

Energy compaction	L1	L2	H1	H2	total energy
ghm	2.1597e+06	9.5831e+05	9.1830e+04	1.4354e+04	3.224e+06
pghm	2.1597e+06	7.3281e+04	9.5680e+03	1.4354e+04	2.257e+06

Energy compaction	L1	H1	H0	total energy
db8	3.1694e+06	3.5377e+04	1.9405e+04	3.224e+06

Table 3: Mean values of the subband energy of ghm, pghm, and db8.

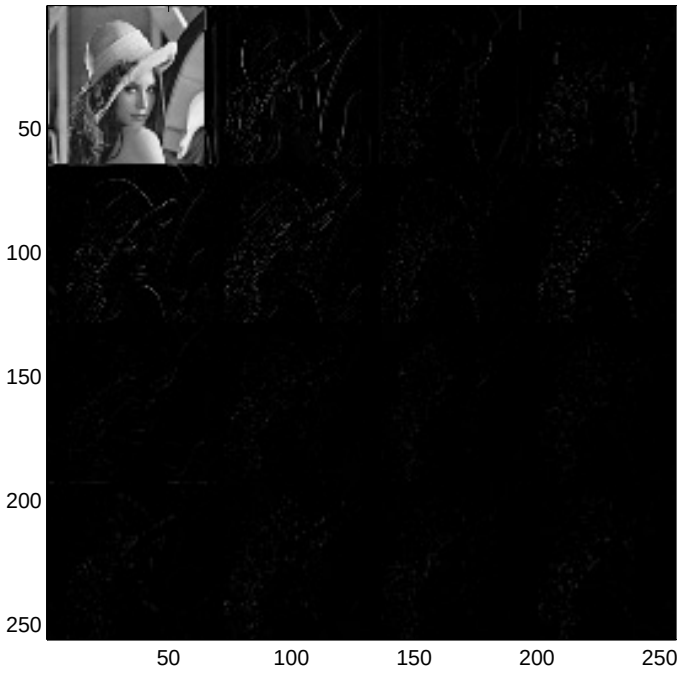

Figure 9: Lena image after GHM multiwavelet transform and inter-band prediction.

	median relative error	median exact error
L1 predict L2	10.39%	9.0903
L1 predict H1	15.32%	4.3674

Table 4: Median values of relative prediction errors.

It is confirmed by Fig. 10 that the smooth region has a better prediction capability than the textured region, since the relative errors in between the 100th and 200th rows are worse than those outside the region. The median values of relative errors are 10.39% and 15.32% for predicted L2 and H1 bands, respectively. Higher relative errors occur for the prediction in the H1 subband. However, this does not imply the exact prediction errors in H1 are larger, since the original errors in H1 are usually smaller. The exact prediction errors of H1 are in fact smaller than that of L2 as given by Table 4 for this test image.

In the second experiment, we would like to compare the magnitude profiles of pghm and db8 filters. We use a series of thresholds 2, 4, 8, 16, 32, 64, etc. to quantize the wavelet coefficients in the transform domain and record the number of symbols below the threshold. In successive approximation coding scheme, all significant symbols of the current quantization layer should be encoded. Thus, if more symbols are insignificant compared to the current threshold, the coding cost of this quantization layer is lower. Here, we use again the Lena image but now treat it as a 2-D signal. A one level 2-D multiwavelet transform and a two level 2-D Daubechies 8-tap transform are performed, and interband prediction is applied to the multiwavelet coefficients.

The magnitude profiles of these two transforms are given in Fig. 11. One can observe a crossover point in Fig. 11. The Db8 filter has more insignificant symbols when the thresholds are below or equal 64, while pghm has more insignificant symbols (and hence lower the coding cost) for a threshold over 64. However, the corresponding bit rates with respect to thresholds over 64 are usually too low for today's practical uses. Thus, prediction can successfully reduce the energy of wavelet coefficients, but energy distribution of prediction residues may not be very compact. Since both the total energy and energy compaction will effect the rate-distortion performance, it is important to reduce the magnitudes of residues or to improve the energy compaction by designing more efficient multiwavelet filters.

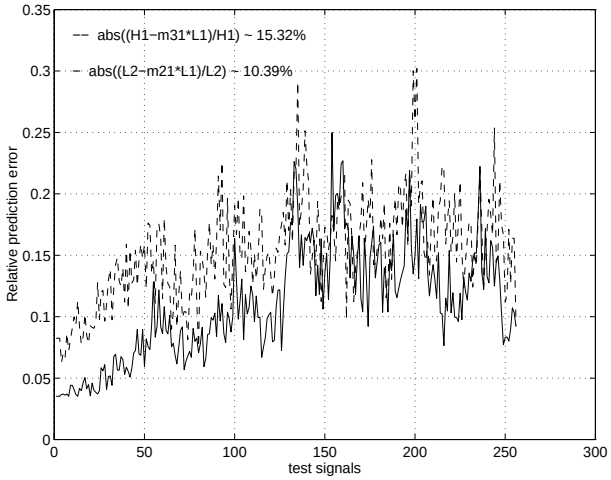

Figure 10: Relative prediction errors for subbands L2 and H1.

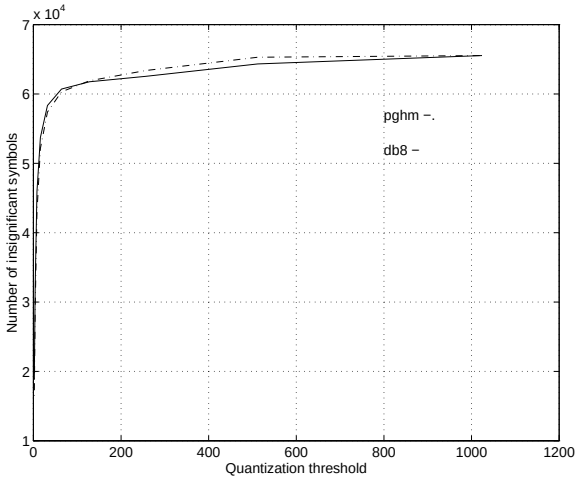

Figure 11: Numbers of insignificant symbols of pghm and db8.

Coding sheme	SNR (dB)	PSNR (dB)	MSE	MAX DIFF	MEAN DIFF
pghm	24.343405	30.007149	8.057174	74.000000	5.762356
db 7-9 tap and LZC	28.432026	34.095772	5.032128	36.838730	3.671435

Table 5: Comparison of image compression results.

5.2 Preliminary Image Compression Result

We compare the performance of our proposed coding scheme with that of LZC [5], which is one of the state-of-the-art coding scheme in this section. The result is highly preliminary since no finetunig has been implemented in our method. The test image is the Lena image of size 512×512. The LZC coding scheme includes the following parts: a 5-level 7-9 tap scalar wavelet transform followed by successive approximation quantizations and embedded wavelet coefficient coding. Our compression method performs a two-level multiwavelet transform, inter-band predictions, successive approximation quantization and embedded coding. The SNR, PSNR, MSE results are reported in Table 5. We see that LZC is still superior to our coding scheme due to a higher efficiency of the Daubechies seven-nine tap filter. However, we expect further improvement of our compression scheme by using other multiwavelets particularly tailored to the compression purpose and vector quantization.

6 CONCLUSION AND EXTENSION

A new image compression technique using an embedded coding of multiwavelet coefficients with subband predictions has been proposed in the paper. We have focused on the the prediction rule across multiwavelet subbands to reduce the redundancy among subbands. How to encode the prediction residues more efficiently using other techniques such as vector quantization and how to improve the energy compaction of the residues with methods such as the multiwavelet packet transform remain to be studied.

7 REFERENCES

[1] J. S. Geronimo, D. P. Hardin, and P. R. Massopust, "Fractal functions and wavelet expansions based on several scaling functions," *J. Approx. Theory*, 1994.

[2] G. Donovan, J. S. Geronimo, D. P. Hardin, and P. R. Massopust, "Construction of orthogonal wavelets using fractal interpolation functions," *preprint*, 1994.

[3] X. G. Xia, J. S. Geronimo, and D. P. Hardin, "Design of prefilters for discrete multiwavelet transforms," *preprint*, 1994.

[4] J. Shapiro, "Embedded image coding using zerotrees of wavelet coefficients," *IEEE Trans. on Signal Processing*, No. 12, pp. 3445–3462, Dec. 1993.

[5] D. Taubman and A. Zakhor, "Multirate 3-D subband coding of video," *IEEE Trans. on Image Processing*, No. 5, pp. 572–588, Sep. 1994.

[6] P.-Y. Cheng, J. Li, and C. C. Kuo, "Scalable Video Coding Using Wavelet Transform and Multiresolution Motion Representation," *SPIE* 1995.

[7] I. Daubechies, *Ten Lectures on Wavelets*, pp. 251–254, SIAM, 1992.